Principal Curvature Guided Surface Geometry Aware Global Shape Representation

Somenath Das and Suchendra M. Bhandarkar
Department of Computer Science, The University of Georgia
Athens, Georgia 30602-7404, USA
somenath@uga.edu, suchi@cs.uga.edu

Abstract

A surface principal curvature preserving local geometry aware global shape representation for 3D shapes is proposed. The shape representation computes the shortest quasi-geodesic path between all possible pairs of points on the shape manifold that enforces minimal variation of geodesic curvature along the path. The normal component of the principal curvature along the quasi-geodesic paths is dominant and shown to preserve the local shape geometry. The eigenspectrum of the proposed representation is exploited to characterize self-symmetry. The commutative property between shape spectra is exploited to compute region-based correspondence between isometric 3D shapes without requiring an initial correspondence map to be specified a priori. The results of the region-based correspondence are extended to characterize the compatibility of the commutative eigen-spectrum in order to address the problem of shape deformation transfer. Eigenspectrum-based characterization metrics are proposed to quantify the performance of the proposed 3D shape descriptor for self-symmetry detection and correspondence determination. The proposed shape descriptor spectrum-based optimization criterion is observed to yield competitive performance compared to relevant state-of-the-art correspondence determination techniques.

Keywords: 3D shape representation, eigenspectrum decomposition, spectrum commutativity, shape correspondence, shape symmetry.

1. Introduction

In Computer Graphics, the study of surface geometry-aware global 3D shape descriptors is critical to enable various 3D shape analysis applications. A desirable quality of a 3D shape descriptor is its ability to discriminate between local regions of a 3D shape, an essential requirement for applications that entail determination of point-wise correspondence between 3D shapes. Ideally, a 3D shape descriptor should demonstrate robustness to local topological noise while effectively capturing the underlying stable shape features that are essential for correspondence determination between 3D shapes. Based on the modality of the underlying shape data (i.e., geometric, topological, etc.) and objective(s) of the application, 3D shape analysis applications can be broadly categorized as purely geometric, semantic or knowledge-driven [1]. Several 3D shape analysis applications drawn from the aforementioned categories typically entail solving a fundamental problem, i.e., one of determining accurate correspondence between the 3D shapes under consideration. Examples of these applications include rigid and non-rigid shape registration [2, 3], shape morphing [4], self-symmetry detection [5], shape deformation transfer [6], 3D surface reconstruction [7], and shape-based object recognition and retrieval [8] among others. The success of these applications is critically dependent on the shape descriptors used for 3D shape correspondence determination. Several of these applications, however, are also dependent upon prior specification of an initial shape correspondence.

We propose a global 3D shape descriptor based on estimation of the approximate geodesic distance between all point pairs on a triangulated mesh-based 3D shape manifold. The 3D shape descriptor represents all the vertices on the 3D shape manifold by their differential coordinates. This allows the geodesics over a 3D shape manifold to be defined as surface curves along which the normal component of the principal curvature is dominant. This property of the geodesics is used to encode the local surface geometry along the curve. The proposed 3D shape descriptor is shown to effectively address the computation of 3D self-symmetry within a shape. The eigenspectrum of the 3D shape descriptor is exploited to address a very important problem, i.e., correspondence determination between isometric 3D shapes (i.e., 3D shapes that are related via an isometric transformation) *without* requiring any prior knowledge about the underlying shapes. Furthermore, the

compatibility of the shape descriptor eigenspectra is formally characterized to generate continuous deformations of a given shape to enable applications such as 3D shape deformation transfer.

On a triangulated 3D surface mesh, the discrete approximation to a geodesic is characterized by an optimal balance of angular distributions over the surface on the either side of the geodesic. These angular distributions are computed in a local neighborhood of each mesh point on the geodesic as depicted in Figure 2 (b) and (c). The balance of the local angular distribution is observed to encode the local geometry of the triangulated mesh along the discrete geodesic. The approximation to a geodesic computed over a discrete 3D triangulated mesh is referred to as a *quasi-geodesic* [9]. The proposed shape descriptor represents the global 3D shape by computing the quasi-geodesic path between all point pairs on the discrete 3D triangulated surface mesh, along which the normal component of the principal curvature is dominant.

We use the eigenspectrum of the global quasi-geodesic-based shape descriptor that encodes that local shape geometry to characterize self-symmetry within a shape and to establish correspondence between isometric deformations of a shape without resorting to any a priori knowledge of the correspondence maps. The all-point-pairs geodesic matrix representation of 3D shapes displays a symmetrical pattern as shown in Figure 1. We employ the eigenspectrum of the symmetrical pattern to detect self-symmetry within a shape. To determine the correspondence between isometric shapes, we exploit the commutative property of the eigenvectors corresponding to the shape descriptor eigenspectrum [10]. The commutative property is shown to demonstrate the approximate orthogonality between different isometric deformations of a discrete triangulated mesh-based 3D shape. Approximate orthogonality refers to the fact that for two distinct eigenvectors ϕ_i and ψ_j chosen from separate shape descriptor eigenspectra, $|\langle \phi_i, \psi_j \rangle| < \epsilon$ where $\langle \cdot, \cdot \rangle$ denotes the scalar inner product of the vector arguments and $\epsilon \approx 0$.

It should be noted that the eigenspectrum of the proposed descriptor is distinct from the well known Laplace-Beltrami eigenspectrum that has been used extensively in several 3D shape analysis and shape synthesis applications. In our case, we exploit the commutative property of the shape descriptor eigenspectrum to establish the correspondence between isometric 3D shapes. It should also be emphasized that, unlike many related approaches [11, 12], the optimization criterion proposed to establish correspondence between isometric 3D shapes does not exploit nor require user-specified initial correspondence maps between the 3D shapes. Furthermore, we extend the correspondence maps detected between isometric shapes to the other isometric deformations of the baseline shapes, with an objective to characterize the compatibility of the correspondence maps to generate smooth deformations of the baseline shapes to enable 3D shape deformation transfer. To the best of our knowledge, the problem of correspondence determination in the absence of prior knowledge of any point-wise mapping between the shapes had not been studied extensively in the research literature.

The remainder of the paper is organized as follows. In Section 2, we present a brief survey of the most relevant works on 3D shape description with an emphasis on the commutative property of isometric shape eigenspectra employed in the proposed correspondence determination scheme. Section 3 describes the specific contributions of our work. The mathematical formulation of the proposed shape descriptor and the associated applications are detailed in Section 4. In Section 5, we present experimental results for 3D self-symmetry detection and characterization, 3D correspondence determination between isometric shapes, and the analysis of compatibility of the commutative eigenspectra used to generate a continuous deformation of a given shape. We conclude in Section 6 with an outline for future work.

2. Background and Related Work

The proposed global shape descriptor is based on the computation of quasi-geodesics between all pairs of points over the discrete triangulated 3D surface mesh where each mesh vertex is represented by its neighborhood-based surface differential. The proposed shape descriptor effectively encodes the local geometry at discrete points over the surface mesh. The eigenspectrum of the descriptor is exploited to address shape self-symmetry, correspondence determination between isometric shapes and the formulation of a metric to characterize generation of smooth deformations of a baseline shape. In this section, we first present a brief survey of some relevant local and global shape descriptors, spectrum-based shape correspondence models and deformation transfer models [1, 13]. We also discuss the principle underlying the commutative property between isometric shape eigenspectra and related work [11] that exploits this principle to determine the correspondence between quasi-isometric shapes.

2.1. Local shape descriptors

The different classes of local shape descriptors can be categorized based on their approach towards the encoding of the underlying local surface geometry. **Ring-based descriptors** typically sample a local surface metric using a parametrically controlled local neighborhood based on *blowing bubbles* [14] or geodesic diameter [15]. Some ring-based descriptors use the local surface normal vectors as surface features computed at discrete points on the surface mesh [16, 17, 18], relative to a superimposed frame of reference over the mesh [19, 20, 21] or in combination

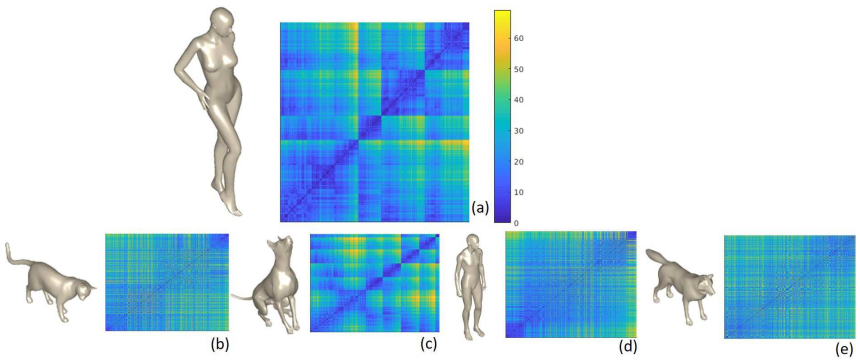

Figure 1. Global representation of 3D shapes using quasi-geodesics computed over a discrete triangulated 3D surface mesh. The 3D shape models shown are (a) *Victoria* (b) *Cat* (c) *Dog* (d) *David* and (e) *Wolf*. The all-point-pairs quasi-geodesic matrix representation of the 3D shapes is observed to be approximately symmetric and the resulting eigenspectrum is observed to preserve self-symmetry over the discrete triangulated 3D mesh-based representation of the 3D shapes.

with local surface curvature [16, 22]. **Expanding descriptors** fit a hypothesis-based parametric model based on features such as geodesic distance [14, 23], volume or surface area [24, 25] to characterize a surface region. Some variants of this descriptor use mesh smoothing [26] or mesh saliency [27] applied over the surface mesh. **Iterative operator-based descriptors** capture the geometric changes within a shape by manipulating the entire mesh surface by employing strategies such as smoothing [26], estimation of local diffusion geometry [28] over the mesh surface, or diffusion based variation [29] within the surface mesh.

2.2. Global shape representation

A global shape representation based upon local surface features is important to effectively characterize the global shape and determine the correspondence between shapes, a fundamental problem in many computer vision and computer graphics applications. Surface descriptors based on the eigenspectrum of the Laplace-Beltrami operator have gained recent popularity in the context of the correspondence problem. Some well known surface descriptors from this class employ a Laplace-Beltrami operator-guided diffusion process that samples a surface metric based on mesh connectivity along the geodesic curves on the 3D surface mesh [29] and diffusion geometry [28] to measure the point-to-point length along a specific path on the surface mesh.

Surface descriptors based on the *heat kernel signature* (HKS) [30, 31, 32] employ the heat diffusion model in conjunction with the eigenspectrum of the Laplace-Beltrami operator to characterize the global shape. The *wave kernel signature* (WKS) [33] employs the principles of quantum mechanics, instead of heat diffusion, in conjunction with the Laplace-Beltrami eigenspectrum to characterize the 3D shape. Smeets et al. [34] present a geodesic distance-based global shape representation that demonstrates robustness to nearly isometric deformations.

2.3. Deformation transfer models

Deformation transfer between shapes [35, 36] is an important application in computer graphics that employs global shape descriptors. The principles of deformation transfer have been employed in many applications such as machine learning-based human motion modeling [37] and sensor-based surface reconstruction [38] to name a few. However, to the best of our knowledge, modeling large-scale deformations using spectral techniques without employing any prior knowledge of correspondence between the shapes has not been explored in detail. In this paper, we propose a metric for characterization of commutative eigenspectra that can quantify the compatibility of the spectra in order to generate smooth deformations of a baseline shape to enable shape deformation transfer.

2.4. Commutative eigenspectrum for correspondence between shapes

Point- or region-based correspondence determination between isometric shapes can be addressed by exploiting the commutative property of the shape descriptor eigenspectrum. In this section we briefly describe the principle underlying the commutative eigenspectra between isometric shapes [10].

2.4.1 Commutative eigenspectrum

Formally, the commutative property implies that given two unitary (i.e., orthogonal) operators Φ_X and Φ_Y defined over an isometric pair of shapes X and Y, one can determine a joint diagonalizer Ψ that diagonalizes both $\Psi^T\Phi_X\Psi$ and $\Psi^T\Phi_Y\Psi$ [10]. The joint diagonalizer Ψ represents the common eigenbases between the isometric shape eigenspectra Φ_X and Φ_Y. Shapes represented as discrete triangulated

meshes need not be exactly isometric to each other due to discretization error. Therefore, in the discrete case, the corresponding shape eigenspectra would be *approximately* commutative. In this paper, the term *"approximately commutative"* is used in the following sense: The eigenspectra Φ_X and Φ_Y of the triangulated shapes X and Y are approximately commutative if $||\Phi_X\Phi_Y - \Phi_Y\Phi_X||_F \approx 0$ where $||\Lambda||_F$ represents the Frobenius norm of matrix Λ.

A detailed treatment of the common eigenbases for approximately commutative spectral operators can be found in [10, 39]. Some recent works [11, 40] employ the commutative principle to formulate a least-squares joint optimization criterion, to extract a common spectral bases that can address correspondence determination between isometric shapes. These applications, however, use prior knowledge of the correspondence to regularize the joint optimization criterion and employ the cotangent discretization scheme for the mesh-based Laplacian [41] to represent the shape operators.

In this paper, we employ the principle of common eigenbases between commutative eigenspectra corresponding to isometric shapes to determine region-wise correspondence. However, in contrast to existing works such as [11], the proposed method employs a novel optimization criterion that does not use any prior knowledge of the correspondence between the shapes under consideration. We elaborate upon the optimization scheme for correspondence determination in Section 4.2.

3. Contributions of the Paper

(1) *Self-symmetry characterization*: We address the problem of self-symmetry detection and characterization by exploiting the eigenspectrum of the proposed global shape descriptor.
(2) *Correspondence determination*: We determine region-wise correspondence between isometric 3D shapes without requiring the user to specify *a priori* an initial point-wise mapping between the two 3D shapes.
(3) *Isometry deformation characterization*: We exploit the results of the region-wise correspondence to formally characterize the extent of isometry deformation between the 3D shapes.
(4) *Compatibility characterization for smooth deformation generation:* We extend the commutative property of the eigenfunctions between baseline shapes to characterize the compatibility of the commutative eigenspectrum in order to address generation of smooth deformations of the baseline shapes.

4. Proposed Shape Operator and Applications

The proposed shape representation for a discrete 3D shape manifold X is denoted by the operator $D_g(X)$, that is computed by determining the quasi-geodesics between all vertex pairs on the discrete manifold X. For the shape representation, we first transform each vertex by its local neighborhood based surface differential so that the i^{th} vertex of shape manifold X is represented by $\delta x_i = x_i - \frac{1}{N}\sum_{y_j \in N(x_i)} y_j$ i.e. the differential coordinate where $N(x_i)$ is the neighborhood of size N for vertex x_i and each $y_j \in N(x_i)$ is a neighboring vertex of x_i. Subsequently, a C^2 function $f : \mathbb{R}^3 \rightarrow \mathbb{R}$ [42, 43] is associated with each vertex $x_i, (1 \leq i \leq n)$ of shape X comprising of n vertices. Consequently, a discrete, triangulated, 3D shape manifold X is represented by the vertices such that $X = \{f(\delta x_1), f(\delta x_2), ..., f(\delta x_n)\}$ where δx_i denotes the surface differential coordinates for the i^{th} vertex of X. The differential transformation ensures that each vertex location also defines the normal to the surface at the vertex as shown in Figure 2 (a). Along a geodesic over a continuous manifold, only the normal component of the principle curvature is dominant compared to it's tangential component. The quasi-geodesic computed for a discrete path $x_i \rightsquigarrow x_j$ minimizes the geodesic distance measure $d(f(\delta x_i), f(\delta x_j))$ between vertices x_i and x_j of X. It should be emphasized that since each vertex x_i is represented by the surface differential coordinates the distance $d(f(\delta x_i), f(\delta x_j))$ represents a path $x_i \rightsquigarrow x_j$ that goes through a geometrically "flat" region over the surface with minimal variation in local geometry between neighboring points on the path. The proposed shape representation $D_g(X)$ records all such quasi-geodesic distances, computed between all vertex-pairs over the surface mesh X. The matrix representation of $D_g(X)$ reveals an implicit symmetrical form, as is evident for the example 3D shapes shown in Figure 1.

For discrete meshes, the computation of geodesics is possible using the stable schemes proposed by Martínez et. al. [9]. The local geometry along a quasi-geodesic over a discrete mesh is preserved as follows. Figure 2 (b) and (c) depicts two scenarios where a probable quasi-geodesic (marked in red) crosses a point P within a neighborhood of triangular mesh facets. In either case, one can measure the discrete geodesic curvature at a point P as follows:

$$\kappa_g(P) = \frac{2\pi}{\theta}(\frac{\theta}{2} - \theta_r) \tag{1}$$

In eqn. (1), θ denotes the sum of all angles formed by the neighborhood of point P. In both the cases, as depicted in Figure 2 (b) and (c), the quasi-geodesics generate angular distributions θ_l and θ_r such that $\theta_l = \sum_i \beta_i$ and $\theta_r = \sum_i \alpha_i$. Since the normal curvature is dominant along the quasi-geodesics, we can compute an optimum balance between θ_l and θ_r that minimizes the discrete geodesic curvature κ_g, which is the tangential component of the curvature along the quasi-geodesic. This optimal balance between angular distributions along a quasi-geodesic encodes

the local angular distribution and hence, the local geometry at surface point P.

To test the robustness of the proposed correspondence scheme we experimented with coarse triangulated meshes. Therefore, to ensure the accurate computation of surface normals at each point of a coarse mesh we considered an additional error correcting scheme explained with an example in Figure 2 (d). Figure 2 (d) depicts a vertex p on the shape manifold with a neighborhood consisting of three vertices q, r and s. As a result, vertex p is shared between three planes defined by disks D_1, D_2 and D_3 with their corresponding normals $\bar{N}_1$, $\bar{N}_2$ and $\bar{N}_3$, respectively. Normals $\bar{N}_1$, $\bar{N}_2$ and $\bar{N}_3$ can be computed from the vertices p, q, r and s. The accuracy of the computed normal direction at a surface point may be severely affected due to the choice of a coarse triangulated mesh. Therefore, the error correcting scheme ensures that the resulting normal $\bar{N}_R$ is constrained to lie within the solid angle region shown in red in Figure 2 (d) that is bounded by normals $\bar{N}_1$, $\bar{N}_2$ and $\bar{N}_3$.

The spectral decomposition of the symmetric shape representation $D_g(X)$ results in the eigenspectrum Φ_X for shape X such that,

$$D_g(X)\Phi_X = \Delta_X \Phi_X \tag{2}$$

where $\Delta_X = \text{diag}(\gamma_1, \gamma_2, ..., \gamma_n)$ denotes the diagonal matrix of eigenvalues $\gamma_i, 1 \leq i \leq n$ and $\Phi_X = \{\Phi_X^1, \Phi_X^2, ..., \Phi_X^n\}$ denotes the eigenvectors $\Phi_X^i, 1 \leq i \leq n$ of shape X with n surface vertices ordered by the corresponding eigenvalues.

4.1. Self-symmetry characterization

We propose the following metric to characterize self-symmetric regions within a shape X. Two regions $X_1, X_2 \subset X$ are possible symmetric regions within X if for some upper bound ε:

$$\left| \sum_{k=1}^{k_0} \Phi_X^k(p) - \sum_{k=1}^{k_0} \Phi_X^k(q) \right|_2 \leq \varepsilon \quad \forall p \in X_1,\ \forall q \in X_2 \tag{3}$$

where $|\cdot|_2$ denotes the $\mathcal{L}^2$ norm. Using spectral analysis one can find a tight bound on ε such that $\varepsilon \leq \sum_{p,q \in X_1,\ r,s \in X_2} |d(p,q) - d(r,s)|_2$ for a C^2 distance metric d [44]. This upper bound on ε is a measure of dissimilarity between regions X_1 and X_2 in terms of the geodesic distances computed between points within the regions. Since the geodesic distances capture the local geometry over the surface, this upper bound, therefore, captures the geometric dissimilarity between regions X_1 and X_2 as well. The parameter ε, aggregated over the entire mesh, indicates the variance of geodesic error computed over the entire shape manifold X. Consequently, ε is a measure of the degree of isometry deformation of X vis-a-vis the baseline shape. We report the bounds on ε computed for different meshes in the Experimental Results section (Section 5). Since the eigenvectors are ordered (in descending order of their eigenvalues) and lower-order eigenvectors (with larger eigenvalues) are known to effectively capture global shape features, we restrict ourselves to the lower-order eigenvectors such that $k_0 \leq 20$ for characterizing self-symmetry. Furthermore, the above characterization can also be used to jointly analyze the region-wise correspondence between two isometric shapes (Section 4.2).

4.2. Correspondence determination between isometric shapes

Determining the compatibility between the eigenbases of isometric shape spectra plays a critical role in applications that entail analysis of multiple 3D shapes; in particular, correspondence determination between 3D shapes. In related work, Ovsjanikov et al. [12] represent the correspondence between two isometric shapes by a parametric map between functional spaces corresponding to the shapes. However, functional map-based methods typically rely on a set of point-wise correspondence maps between shapes provided a priori for optimization of the correspondence criterion [12, 45]. In contrast, the proposed approach does not assume knowledge of any prior correspondence mapping between the shapes under consideration.

For correspondence determination between two isometric shapes X and Y we exploit the fact that the eigendecomposition of symmetric shape operators $D_g(X)$ and $D_g(Y)$ leads to approximately commutative eigenspectra Φ_X and Φ_Y respectively. The characterization *"approximately commutative"* is on account of the triangulated discretization of the surface meshes describing the shapes and follows the formal definition given in Section 2.4.

We couple Φ_X and Φ_Y by the commutative terms $\Phi_X^T \Delta_Y \Phi_Y$ and $\Phi_Y^T \Delta_X \Phi_X$ to solve the following optimization problem:

$$\bar{\Phi}_X, \bar{\Phi}_Y = \underset{\phi_x, \phi_y}{\text{argmin}} \left\{ |\phi_x^T \Delta_Y \phi_y|_F + |\phi_y^T \Delta_X \phi_x|_F \right\} \tag{4}$$

where $\phi_x \subset \Phi_X$, $\phi_y \subset \Phi_Y$; Δ_X, Δ_Y are diagonal matrices of eigenvalues (eqn. (2)) corresponding to shapes X and Y, respectively and $|\cdot|_F$ denotes the Frobenius norm. The optimization in eqn. (4) considers all pairs of subsets of eigenvectors $\{1, \ldots, k_0\}$ from the eigenspectra of shapes X and Y. It should be noted that eqn. (4) does not require that *a priori* correspondence maps be specified. The optimized maps $\bar{\Phi}_X$ and $\bar{\Phi}_Y$ over shapes X and Y encode the corresponding regions between them where corresponding regions are denoted by the same color (generated using a standard colormap library).

From the optimized maps $\bar{\Phi}_X$ and $\bar{\Phi}_Y$, the relative correspondence error between shapes X and Y is given by met-

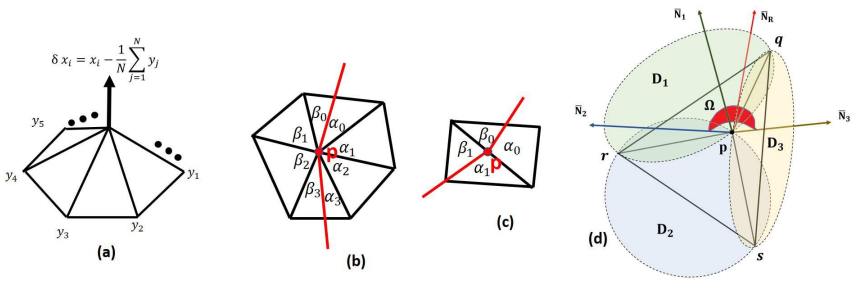

Figure 2. The proposed shape descriptor represents each vertex of the mesh by the discrete differential coordinates. (a) The resulting coordinate axis aligns with the normal on the surface at the vertex. Vertices y_j's belong to the neighborhood ring $N(x_i)$ of vertex x_i. (b) and (c) depicts two possible crossings of a geodesic at a point P on the surface. The balance between left and right angular distributions $\theta_l = \sum_i \beta_i$ and $\theta_r = \sum_i \alpha_i$ generated by a geodesic at point P on the surface mesh encode the local geometry of the discrete surface mesh at P. For coarse meshes, an additional scheme depicted in (d) is considered to ensure the accuracy of the surface normal computation. This scheme ensures that the resultant normal $\bar{N}_R$ is constrained to lie within the region in red defined by the disc normals $\bar{N}_1$, $\bar{N}_2$ and $\bar{N}_3$.

ric $C_{X,Y} = \sum_{k=1}^{k_0} |\bar{\Phi}_X^k - \bar{\Phi}_Y^k|_2$. To compute $C_{X,Y}$ we consider the lower-order eigenvectors by setting $k_0 \leq 20$. It is to be noted that $C_{X,Y}$ essentially represents the geometric difference due to isometric transformations between corresponding regions of shapes X and Y as captured by the spectrum of the shape representations. Thus, $C_{X,Y}$ is a measure of the degree of *isometric deformation* between shapes X and Y.

4.3. Compatibility of the commutative spectrum for deformation transfer

The proposed global shape descriptor is designed to encode the local surface geometry that can be used to establish correspondence between isometric deformations of a shape following commutative optimization as explained in Section 4.2. Based on this property of the descriptor, we hypothesize that the commutative spectra can be successfully utilized to generate all continuous deformations of a shape X from initial correspondence between two isometric deformations of X. The experimental setup for testing the hypothesis is explained in Figure 3. The experiment first computes the commutative eigenspectra $\bar{\Phi}_1, \bar{\Phi}_2$ of two baseline isometric deformations S_1 and S_2 of a shape category following the optimization in eqn. (4). The optimized eigenspectra are then mapped on a set S, consisting of other isometric deformations $S_3, S_4, \ldots$ etc. of the baseline shape.

We propose the following metric that evaluates the correspondence established by the commutative eigenspectra $\bar{\Phi}_1, \bar{\Phi}_2$ between all shape pairs $\{S_i, S_j\}$ from set S:

$$D(S) = \frac{1}{|S|} \sum_{\substack{S_i, S_j \in S \\ i \neq j}} C_{S_i, S_j} \tag{5}$$

where $|S|$ is the size of the set S and C_{S_i,S_j} is the correspondence error between shapes S_i and S_j as described in Section 4.2. This quantitative characterization $D(S)$ (eqn. (5)) is suggestive of whether the commutative shape descriptor spectrum of the baseline shapes can address correspondence between baseline shapes and other isometric deformations of the shape category. This characterization can be useful to effectively address the problem of deformation transfer [6, 35, 36].

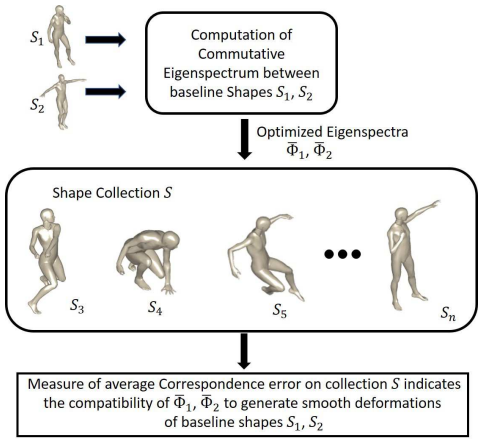

Figure 3. Characterization of compatibility of a commutative eigenspectrum to address continuous deformation of baseline shapes.

5. Experimental Results

For our experiments we have chosen the TOSCA dataset consisting of eleven non-rigid shape categories, i.e., *Cat*, *Dog*, *Wolf*, two *Human Males*, *Victoria*, *Gorilla*, *Horse*, *Centaur*, *Lioness* and *Seahorse* [46]. Within each shape category, the individual shapes represent different transformations of the baseline shape such as isometry, isometry coupled with topology change and different mesh triangulations, among others, of the baseline shape. In this work, we consider shapes that differ via an isometry transformation.

Some examples of isometry transformations of shapes are shown in Figure 4. Experimental results of each of the applications are formally described in Sections 5.1, 5.2 and 5.3 using visual validation of the results followed by the corresponding numerical evaluations. We have experimented with coarse meshes that are reduced by more than 87% of their original size or resolution. The results of the proposed shape representation are compared with those from relevant state-of-the-art shape representation schemes. The compatibility of the commutative eigenspectra to address deformation transfer is visually validated in Section 5.3.

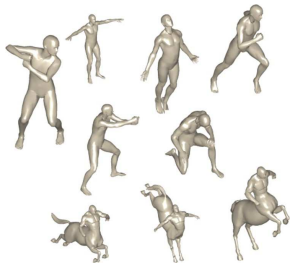

Figure 4. Examples of isometry transformation for the shape categories *Human Male* and *Centaur* from the TOSCA dataset.

5.1. 3D self symmetry detection

Figure 5 presents the self-symmetry maps obtained for different shape categories using eqn. (3). The maps in Figure 5 correspond to the second eigenvector Φ_X^2 obtained from the spectral decomposition of the global operator $D_g(X)$ for each shape. Table 1 presents the self-symmetry characterization measure, denoted by the upper bound ε in eqn. (3), for each shape category. This characterization measure represents the deformation between symmetric regions within a shape that the characterization criteria would be able to address as explained in Section 4.1.

5.2. 3D correspondence determination

Since the lower-order eigenvectors represent global shape geometry more accurately, we consider the first 20 eigenvectors to compute the global region-based correspondence between the isometric shapes. Figure 6 shows the results of correspondence determination between the isometric *Human Male* shapes obtained via the optimization criterion described in eqn. (4). Except for a small region at lower left leg, correspondence maps between the shapes are shown to be consistent across eigenvectors of different order. It is to be noted that the eigenmaps for a single shape across different order of eigenvectors are very similar to each other as well. In Figure 6, eigenvectors up to order 9 are shown to demonstrate this consistency both within a shape and between shapes. This provides experimental validation of the fact that the proposed descriptor spectrum effectively captures a global invariance within a shape that is robust to isometric transformations.

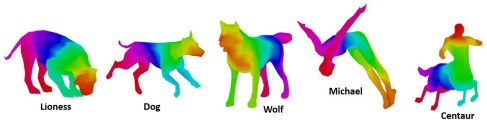

Figure 5. Self-symmetry detection for five different shape categories using the spectrum of the global representation $D_g(X)$ for the shape X. Each map corresponds to the second eigenvector Φ_X^2 of the shape operator spectrum.

Table 1. Self-symmetry characterization measure for different shape categories in the TOSCA dataset. The average degree of isometry transformation within the category *Seahorse* is observed to be at least 19% higher than the other categories.

Category	ε	Category	ε
Lioness	0.0506	*Dog*	0.0486
Wolf	0.0485	*Michael*	0.0486
Seahorse	0.0603	*Centaur*	0.0485

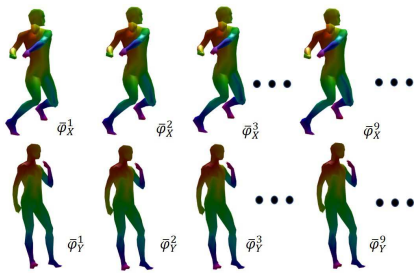

Figure 6. Pairwise consistency between corresponding eigenmaps on the isometric deformations of the *Human Male* shapes. For correspondence estimation, the optimization criterion described in eqn. (4) is used. Lower-order eigenvectors are considered for correspondence estimation since they effectively capture the global shape geometry. Maps across different order of eigen vectors on the same shape also demonstrate high degree of consistency.

Table 2. Comparison of average relative correspondence error $C_{X,Y}$ between [47] and the proposed method for correspondence determination between isometric shapes across different shape categories.

Category	Average $C_{X,Y}$ for [47]	Average $C_{X,Y}$ for present approach
Victoria	0.069	0.045
Dog	0.0624	0.0474
Cat	0.06	0.0522
Michael	0.057	0.0363
Horse	0.0559	0.0179
Centaur	0.052	0.0261

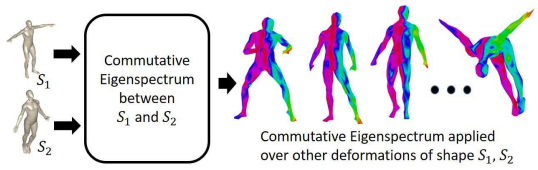

Figure 7. Experimental setup to characterize the effectiveness of commutative eigenspectrum for generating smooth deformations of a baseline shape. The results for *Human* models are shown.

The relative correspondence error for these maps can be characterized by the measure $C_{X,Y}$ defined in Section 4.2. Table 2 lists this measure for isometric shapes from different shape categories. Lower $C_{X,Y}$ values denote a higher degree of correspondence accuracy achieved via the optimization described in eqn. (4). We compare our method with recent work [47] where the shape representation is based upon geodesics between mesh vertices described using a Cartesian coordinate system. The proposed method shows significant improvement since the differential representation of the shape vertices capture the local geometry and topology variations more effectively. We emphasize here, that the correspondence accuracy is achieved without requiring any prior mapping between the shapes.

5.3. Deformation transfer compatibility characterization

Following the experimental setup described in Figure 3 we tested the compatibility of commutative eigenspectra to address deformation transfer on various shape categories. One such experiment on the *Human* model is described in Figure 7. The experiment first computes the commutative eigenspectra following the optimization in eqn. (4) on baseline shapes S_1 and S_2 as shown in Figure 7. Subsequently, the optimized eigenspectra are mapped over different isometric deformations of shapes S_1 and S_2. The visual similarity of the maps suggest that the optimized eigenspectra can be effectively used to generate smooth deformations of baseline shapes and thus can be effectively employed for deformation transfer for the shape category [35].

The quantitative characterization of this compatibility can be computed using eqn. (5). We observed that this metric for different shape categories followed closely the characterization metric depicted in Table 2 and was hence not tabulated in this section to avoid redundancy. Table 3 compares the performance of the proposed representation scheme with the performance of other state-of-the-art representation schemes [47, 48, 49]. Methods [48, 49] were further combined with the functional map technique [12] in order to improve their correspondence accuracy via functional map-based local refinement. The results of correspondence for these combined approaches are also presented in Table 3. The numerical values presented in Table 3 denote the highest percentage correspondence accuracy achieved by the various representation schemes along with the corresponding average geodesic error. The performance of the proposed representation scheme is observed to compare very well with the performance of the other state-of-the-art representation schemes. These results underscore the central hypothesis underlying the proposed shape representation, namely that competitive performance in self-symmetry detection and characterization, and correspondence map determination between isometric 3D shapes can be achieved by the proposed shape representation without requiring prior knowledge of correspondence mapping between the shapes in contrast to other state-of-the-art correspondence determination techniques [48, 49].

Table 3. Comparison between the proposed scheme and other state-of-the-art schemes described in [47], [48] and [49]. Correspondence results from methods [48], [49] combined with functional maps [12] are also compared.

Methods	Geodesic Error	% Correspondence
[48]	0.11	~ 95
[12] and [48]	0.06	~ 95
[49]	0.25	~ 90
[12] and [49]	0.2	~ 90
[47]	0.15	~ 94
Proposed Scheme	0.27	~ 94.55

6. Conclusions and Future Work

In this paper we proposed a global shape representation scheme using quasi-geodesics computed over the entire discrete shape manifold where each vertex of the manifold is represented by its neighborhood-based surface differential coordinates. The spectral decomposition of this representation is used to identify self-symmetric regions of the shape. By exploiting the commutative property of the eigenbases of the proposed representation, we successfully computed region-wise correspondence between isometric shapes and compared the results to those from state-of-the-art correspondence models. Furthermore, we investigated the effectiveness of the commutative eigenspectra to address smooth deformation transfer between 3D shapes. We also proposed formal metrics for characterization of self-symmetry identification and correspondence determination.

A key contribution of this work is the fact that no prior mappings between shapes was exploited for correspondence and self-symmetry determination. As an extension of the current scheme, we intend to apply the shape representation model, combined with functional maps [12] to address applications such as deformation transfer between isometric shapes in absence of any prior knowledge, and for correspondence determination between near-isometric shapes [11].

References

[1] O. Van Kaick, H. Zhang, G. Hamarneh, and D. Cohen-Or, "A survey on shape correspondence," *Computer Graphics Forum*, vol. 30, no. 6, pp. 1681–1707, 2011. 1, 2

[2] W. Chang and M. Zwicker, "Automatic registration for articulated shapes," *Computer Graphics Forum*, vol. 27, no. 5, pp. 1459–1468, 2008. 1

[3] N. Gelfand, N. J. Mitra, L. J. Guibas, and H. Pottmann, "Robust global registration," *Symposium on Geometry Processing*, vol. 2, no. 3, p. 5, 2005. 1

[4] V. Kraevoy and A. Sheffer, "Cross-parameterization and compatible remeshing of 3D models," *ACM Transactions on Graphics (TOG)*, vol. 23, no. 3, pp. 861–869, 2004. 1

[5] R. Gal and D. Cohen-Or, "Salient geometric features for partial shape matching and similarity," *ACM Transactions on Graphics (TOG)*, vol. 25, no. 1, pp. 130–150, 2006. 1

[6] R. W. Sumner and J. Popović, "Deformation transfer for triangle meshes," *ACM Transactions on Graphics (TOG)*, vol. 23, no. 3, pp. 399–405, 2004. 1, 6

[7] Y. Pekelny and C. Gotsman, "Articulated object reconstruction and markerless motion capture from depth video," *Computer Graphics Forum*, vol. 27, no. 2, pp. 399–408, 2008. 1

[8] V. Jain and H. Zhang, "A spectral approach to shape-based retrieval of articulated 3D models," *Computer Aided Design*, vol. 39, no. 5, pp. 398–407, 2007. 1

[9] D. Martínez, L. Velho, and P. C. Carvalho, "Computing geodesics on triangular meshes," *Computers & Graphics*, vol. 29, no. 5, pp. 667–675, 2005. 2, 4

[10] J.-F. cois Cardoso, "Perturbation of joint diagonalizers." 2, 3, 4

[11] A. Kovnatsky, M. M. Bronstein, A. M. Bronstein, K. Glashoff, and R. Kimmel, "Coupled quasi-harmonic bases," *Computer Graphics Forum*, vol. 32, no. 2pt4, pp. 439–448, 2013. 2, 4, 8

[12] M. Ovsjanikov, M. Ben-Chen, J. Solomon, A. Butscher, and L. Guibas, "Functional maps: a flexible representation of maps between shapes," *ACM Transactions on Graphics (TOG)*, vol. 31, no. 4, p. 30, 2012. 2, 5, 8

[13] P. Heider, A. Pierre-Pierre, R. Li, and C. Grimm, "Local shape descriptors, a survey and evaluation," *Proceedings of the 4th Eurographics Conference on 3D Object Retrieval*, pp. 49–56, 2011. [Online]. Available: http://dx.doi.org/10.2312/3DOR/3DOR11/049-056 2

[14] M. Mortara, G. Patané, M. Spagnuolo, B. Falcidieno, and J. Rossignac, "Blowing bubbles for multi-scale analysis and decomposition of triangle meshes," *Algorithmica*, vol. 38, no. 1, pp. 227–248, 2004. 2, 3

[15] H. Pottmann, J. Wallner, Q.-X. Huang, and Y.-L. Yang, "Integral invariants for robust geometry processing," *Computer Aided Geometric Design*, vol. 26, no. 1, pp. 37–60, 2009. 2

[16] T. Gatzke, C. Grimm, M. Garland, and S. Zelinka, "Curvature maps for local shape comparison," *Proceedings of the International Conference on Shape Modeling and Applications*, pp. 244–253, 2005. 2, 3

[17] F. Stein and G. Medioni, "Structural indexing: Efficient 3-D object recognition," *IEEE Transactions on Pattern Analysis & Machine Intelligence*, no. 2, pp. 125–145, 1992. 2

[18] J. L. Ong and A.-K. Seghouane, "From point to local neighborhood: polyp detection in ct colonography using geodesic ring neighborhoods," *IEEE Transactions on Image Processing*, vol. 20, no. 4, pp. 1000–1010, 2011. 2

[19] S. M. Yamany and A. A. Farag, "Free-form surface registration using surface signatures," *The Proceedings of the Seventh IEEE International Conference on Computer Vision*, vol. 2, pp. 1098–1104, 1999. 2

[20] C. S. Chua and R. Jarvis, "Point signatures: A new representation for 3D object recognition," *International Journal of Computer Vision*, vol. 25, no. 1, pp. 63–85, 1997. 2

[21] S. M. Yamany and A. A. Farag, "Surface signatures: an orientation independent free-form surface representation scheme for the purpose of objects registration and matching," *IEEE Transactions on Pattern Analysis and Machine Intelligence*, vol. 24, no. 8, pp. 1105–1120, 2002. 2

[22] J. Ong and A.-K. Seghouane, "From point to local neighborhood: Polyp detection in ct colonography using geodesic ring neighborhoods," *IEEE Transactions on Image Processing*, vol. 20, no. 4, pp. 1000–1010, April 2011. 3

[23] G. Cipriano, G. N. Phillips, and M. Gleicher, "Multi-scale surface descriptors," *IEEE Transactions on Visualization and Computer Graphics*, vol. 15, no. 6, pp. 1201–1208, 2009. 3

[24] M. L. Connolly, "Measurement of protein surface shape by solid angles," *Journal of Molecular Graphics*, vol. 4, no. 1, pp. 3–6, 1986. 3

[25] H. Pottmann, J. Wallner, Q.-X. Huang, and Y.-L. Yang, "Integral invariants for robust geometry processing," *Computer Aided Geometric Design*, vol. 26, no. 1, pp. 37–60, 2009. 3

[26] X. Li and I. Guskov, "Multiscale features for approximate alignment of point-based surfaces." *Proceedings of Symposium on Geometry Processing*, vol. 255, pp. 217–226, 2005. 3

[27] C. H. Lee, A. Varshney, and D. W. Jacobs, "Mesh saliency," *ACM Transactions on Graphics (TOG)*, vol. 24, no. 3, pp. 659–666, Jul. 2005. [Online]. Available: http://doi.acm.org/10.1145/1073204.1073244 3

[28] A. M. Bronstein, M. M. Bronstein, R. Kimmel, M. Mahmoudi, and G. Sapiro, "A Gromov-Hausdorff framework with diffusion geometry for topologically-robust non-rigid shape matching," *International Journal of Computer Vision*, vol. 89, no. 2-3, pp. 266–286, 2010. 3

[29] R. M. Rustamov, "Laplace-Beltrami eigenfunctions for deformation invariant shape representation," *Proceedings of the Fifth Eurographics Symposium on Geometry Processing*, pp. 225–233, 2007. 3

[30] J. Sun, M. Ovsjanikov, and L. Guibas, "A concise and provably informative multi-scale signature based on heat diffusion," *Computer Graphics Forum*, vol. 28, no. 5, pp. 1383–1392, 2009. 3

[31] M. M. Bronstein and I. Kokkinos, "Scale-invariant heat kernel signatures for non-rigid shape recognition," *Proceedings of IEEE Conference on Computer Vision and Pattern Recognition (CVPR)*, pp. 1704–1711, 2010. 3

[32] D. Boscaini, J. Masci, E. Rodolà, M. M. Bronstein, and D. Cremers, "Anisotropic diffusion descriptors," *Computer Graphics Forum*, vol. 35, no. 2, pp. 431–441, 2016. 3

[33] M. Aubry, U. Schlickewei, and D. Cremers, "The wave kernel signature: A quantum mechanical approach to shape analysis," *Proceedings of IEEE International Conference on Computer Vision Workshops (ICCV Workshops)*, pp. 1626–1633, 2011. 3

[34] D. Smeets, J. Hermans, D. Vandermeulen, and P. Suetens, "Isometric deformation invariant 3D shape recognition," *Pattern Recognition*, vol. 45, no. 7, pp. 2817–2831, 2012. 3

[35] B. Lévy, "Laplace-beltrami eigenfunctions towards an algorithm that " understands" geometry," in *Shape Modeling and Applications, 2006. SMI 2006. IEEE International Conference on*. IEEE, 2006, pp. 13–13. 3, 6, 8

[36] R. W. Sumner, M. Zwicker, C. Gotsman, and J. Popović, "Mesh-based inverse kinematics," *ACM transactions on graphics (TOG)*, vol. 24, no. 3, pp. 488–495, 2005. 3, 6

[37] G. Pons-Moll, J. Romero, N. Mahmood, and M. J. Black, "Dyna: A model of dynamic human shape in motion," *ACM Transactions on Graphics (TOG)*, vol. 34, no. 4, p. 120, 2015. 3

[38] M. Zollhöfer, M. Nießner, S. Izadi, C. Rehmann, C. Zach, M. Fisher, C. Wu, A. Fitzgibbon, C. Loop, C. Theobalt *et al.*, "Real-time non-rigid reconstruction using an rgb-d camera," *ACM Transactions on Graphics (TOG)*, vol. 33, no. 4, p. 156, 2014. 3

[39] A. Yeredor, "Non-orthogonal joint diagonalization in the least-squares sense with application in blind source separation," *IEEE Transactions on Signal Processing*, vol. 50, no. 7, pp. 1545–1553, 2002. 4

[40] A. Kovnatsky, M. M. Bronstein, X. Bresson, and P. Vandergheynst, "Functional correspondence by matrix completion," *Proceedings of the IEEE Conference on Computer Vision and Pattern Recognition (CVPR)*, pp. 905–914, 2015. 4

[41] M. Meyer, M. Desbrun, P. Schröder, and A. H. Barr, "Discrete differential-geometry operators for triangulated 2-manifolds," *Visualization and Mathematics III*, pp. 35–57, 2003. 4

[42] O. Azencot, S. Weißmann, M. Ovsjanikov, M. Wardetzky, and M. Ben-Chen, "Functional fluids on surfaces," *Computer Graphics Forum*, vol. 33, pp. 237–246, 2014. 4

[43] J. Martinez Esturo, C. Rössl, and H. Theisel, "Smoothed quadratic energies on meshes," *ACM Transactions on Graphics (TOG)*, vol. 34, no. 1, p. 2, 2014. 4

[44] N. Dunford and J. T. Schwartz, *Linear operators: Part II: Spectral Theory: Self Adjoint Operators in Hilbert Space*. Interscience Publishers, 1963. 5

[45] A. Nguyen, M. Ben-Chen, K. Welnicka, Y. Ye, and L. Guibas, "An optimization approach to improving collections of shape maps," *Computer Graphics Forum*, vol. 30, pp. 1481–1491, 2011. 5

[46] M. Ovsjanikov, A. M. Bronstein, M. M. Bronstein, and L. J. Guibas, "Shape Google: a computer vision approach to isometry invariant shape retrieval," pp. 320–327, 2009. 6

[47] S. Das and S. M. Bhandarkar, "Local geometry inclusive global shape representation," *Proceedings of IEEE International Conference on Computer Vision Workshops (ICCV Workshops)*, pp. 1256–1265, 2017. 7, 8

[48] V. G. Kim, Y. Lipman, and T. Funkhouser, "Blended intrinsic maps," *ACM Transactions on Graphics (TOG)*, vol. 30, no. 4, pp. 79:1–79:12, 2011. 8

[49] Y. Sahillioglu and Y. Yemez, "Coarse-to-fine combinatorial matching for dense isometric shape correspondence," *Computer Graphics Forum*, vol. 30, no. 5, pp. 1461–1470, 2011. 8